JOURNAL OF MATERIALS SCIENCE 19 (1984) 1283–1295

Oxidation mechanism of porous silicon nitride

F. PORZ, F. THÜMMLER
Institut für Werkstoffkunde II, Universität Karlsruhe, Institut für Material- und Festkörperforschung, Kernforschungszentrum Karlsruhe, West Germany

The oxidation of reaction-bonded silicon nitride (RBSN) has been studied in air between 800 and 1500° C. The extent of internal oxidation is governed by the radius of the pore channels allowing the oxygen to penetrate the specimen. The velocity of oxygen transport into narrow channels is very low compared to the reaction rate of oxygen with Si_3N_4. Because of these two concurrent processes an oxygen gradient is built up along the channel axis leading to SiO_2 formation mainly at the channel mouth. The typical oxidation isotherm of RBSN is represented by an asymptotic law. The mass gain and the penetration depth of oxidation is calculated, based on reaction-rates of Si_3N_4-powder, oxygen-diffusion-data and the pore-characteristics of the RBSN-materials, and compared with the experimental results. The results clearly indicate, that high quality RBSN may wel be used in oxidizing atmosphere without extensive internal oxidation.

1. Introduction

Silicon nitride is a most interesting ceramic material because of its promising thermomechanical properties. One variety of silicon nitride is the reaction-bonded silicon nitride (RBSN), which typically has a porosity af approximately 15 vol%. Thus the level of the mechanical properties at room temperature is not particularly outstanding, but the strength is retained up to very high temperatures and creep properties are excellent. This is especially the case for materials which do not undergo severe internal oxidation [1, 2]. Silicon nitride is thermodynamically unstable with respect to oxidation in air. Under current oxidizing conditions, with high oxygen partial pressure, a protective SiO_2 surface layer is built up leading to a parabolic rate law. The growth of SiO_2 films on Si_3N_4 proceeds via diffusion of oxygen through the oxide. Several investigations into the oxidation of pure Si_3N_4 (powder and CVD material) have been published, a review is given in [3]. The parabolic rate coefficients are plotted in the Arrhenius diagram shown in Fig. 1.

The numbers indicate the apparent activation energies in kJ mol^{-1}. The widely different results are due to the fact that in most cases the reduction of surface area due to blocking of pores in the powder particles and in the powder bed has not been properly taken into account [3]. This leads to the surprising result of higher oxidation rates of CVD-materials as for powders. Only the values of Tétard *et al.* [5] are higher than those for the CVD Si_3N_4. The comparison of Tétard's parabolic rate coefficients and the activation energy with the oxygen diffusion data is good [3, 14]; one can assume these to be the most valuable data.

The oxidation behaviour of RBSN considerably differs from that of dense Si_3N_4 materials or powders because of the inherent open porosity. During the very first investigations, it was found, that RBSN exhibits a rapid mass increase in the first two hours of oxidation at 1200° C but no additional mass increase after 80 h [15]; it was suggested that a protective film forms on the surface, so preventing further oxidation [16].

The oxidation of RBSN occurs in two distinguished stages as first described by Davidge *et al.* [17]. During the first stage external and internal surfaces of the porous material are oxidized. When the radii of the pore channels, allowing the oxygen to diffuse into the specimens, are narrowed by the SiO_2 layer formed on the walls of the channels, the internal oxidation ceases and in the second stage only the outer surface of the specimens is oxidized further.

Several studies of the oxidation of RBSN have

0022–2461/84 $03.00 + .12

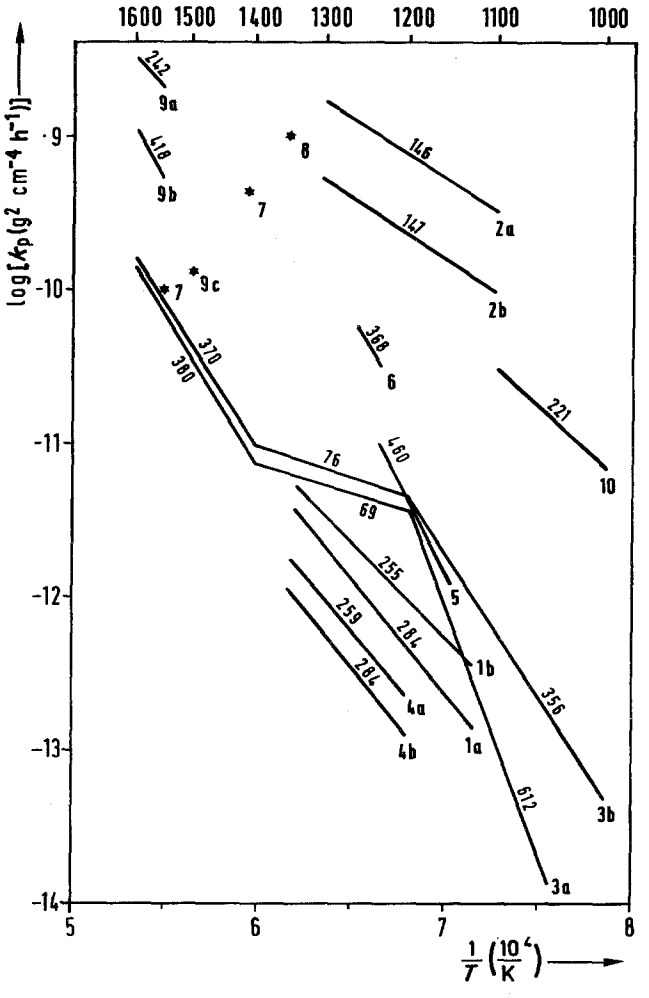

Figure 1 Parabolic rate coefficients and activation energies for the oxidation of Si_3N_4. (Numbers at the slope indicate activation energy in kJ mol^{-1}.) Curve 1a, air [4]; curve 1b, oxygen [4]; curve 2a, oxygen, $\alpha/\beta = 2$ [5]; curve 2b, oxygen, $\alpha/\beta = 1.4$ [5]; curve 3a, air [6]; curve 3b, oxygen [6]; curve 4a, air, α [7]; curve 4b, air, β [7]; curve 5, air [8]; curve 6, oxygen [9]; points 7, air [10]; point 8, air [11]; curve 9a, oxygen, α [12]; curve 9b, oxygen, amorphous [12]; point 9c, air, α [12]; curve 10, oxygen [13]; curves 1 to 5, Si_3N_4 powder; curves 6 to 10 CVD Si_3N_4.

been made covering the temperature range from 800 to 1600° C and up to 5000 h oxidation [6, 17–24]. In these studies the typical two stage oxidation pattern has been confirmed. The comparison of the results is difficult, because of the widely differing materials and different heating conditions. Mass gains of up to 20% have been reported [22]. The duration of the first oxidation stage varies, for example, from 25 min [17] up to 240 min [18] at 1200° C; for details see [3]. It has been shown, that the amount of internal oxidation is strongly dependent on the annealing conditions (heating rate and temperature) and on the microstructure (porosity and pore size distribution) of the RBSN qualities [3, 23].

Up to now, the reason why the typical RBSN oxidation behaviour with the two stage process and only small outer oxidized regions of the specimens occurs, has not yet been sufficiently clarified. The aim of this paper is to describe the oxidation behaviour of RBSN not only in a qualitative but also in a quantitative manner.

2. Characterization of the RBSN materials

For the experiments described, two RBSN qualities with rather different density, open porosity and pore channel radii have been chosen (Table I). The open porosity and the volume distribution of the porosity have been measured with the aid of mercury porosimetry. Mercury behaves as a non-wetting liquid and one must apply pressure to make it penetrate into the openings of a porous body. The registration of the pressure and the mercury volume intruded, or on releaving the pressure, extruded from the sample, leads to volume distributions as shown in Fig. 2.

Because of the typical nature of porosity in RBSN, small channels linking larger pores, a marked hysteresis is observed. The mercury which penetrates the large pores via fine channels on

TABLE I Characteristics of the RBSN materials

Properties	Material	
	A	B
density ($g\,cm^{-3}$)	2.47	2.63
open porosity (vol %)	21	14
mean pore channel radius (nm)	108	50
specific surface area (m^2g^{-1})	1.1	2.4
α/β-Si_3N_4 ratio	80/20	90/10
impurities		
Fe	0.38	0.34
Al	0.23	0.18
Ca	0.05	0.04
Mg	0.04	0.02

intrusion is unable to extrude completely. The intrusion curve gives the volume that is accessible through openings of a certain radius. From the extrusion curve the distribution of the channel volume is obtained [25]. The radii of these channels, which allow oxygen to penetrate the material during oxidation, determine the oxidation behaviour. For this reason the radius at 50% of the extruded mercury volume is given in Table I as mean pore channel radius. The open porosity was calculated from the total amount of mercury that penetrated the specimen.

The determination of the internal surface area of RBSN was performed through the measurement of low-temperature nitrogen adsorption. The amount of crystalline phases has been determined by X-ray diffraction. The specific surface area of material B is about twice that of material A because of the narrower pore channels in material B. Both qualities contain mostly α-Si_3N_4, the amount of metallic impurities differs only slightly.

3. Oxidation of RBSN

3.1. Experimental results

Oxidation tests were conducted in a thermal balance using specimens with the dimensions 12 mm x 12 mm x 3.5 mm. All faces were ground. To avoid oxidation during heating, the specimens were heated in dry nitrogen to the test temperature, then $10\,l\,h^{-1}$ of dried air was passed across the specimens.

The measured oxidation isotherms for both materials are shown in Figs. 3a and b, and 4a and b for short and long oxidation times, respectively, for temperatures of 800 to 1500° C. The mass gain is related to the original mass of the specimens.

Normally one plots the mass gain related to the surface area; this is not adequate for the oxidation of RBSN, because the "true" surface area, which is actually involved in the oxidation process, is not known. The isotherms exhibit the typical pattern for RBSN materials with a high initial oxidation rate which than falls off rapidly towards longer oxidation times.

3.2. Parabolic treatment

The oxidation of silicon-based materials usually follows a linear parabolic relationship as is described in detail for the silicon oxidation by Deal and Grove [26]. This can be written in the form

$$\left(\frac{\Delta m}{S}\right)^2 + \frac{k_p}{k_l}\left(\frac{\Delta m}{S}\right) = k_p t \qquad (1)$$

with the surface S, the parabolic and linear rate coefficients k_p and k_l, respectively, and the oxidation time t. The linear oxidation behaviour is observed for a short initial period, then the oxi-

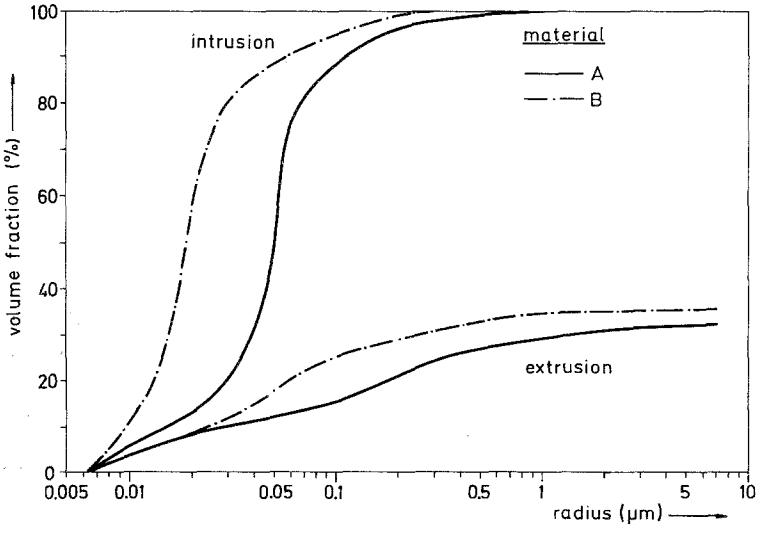

Figure 2 Distribution of open porosity in RBSN measured during intrusion and extrusion of mercury.

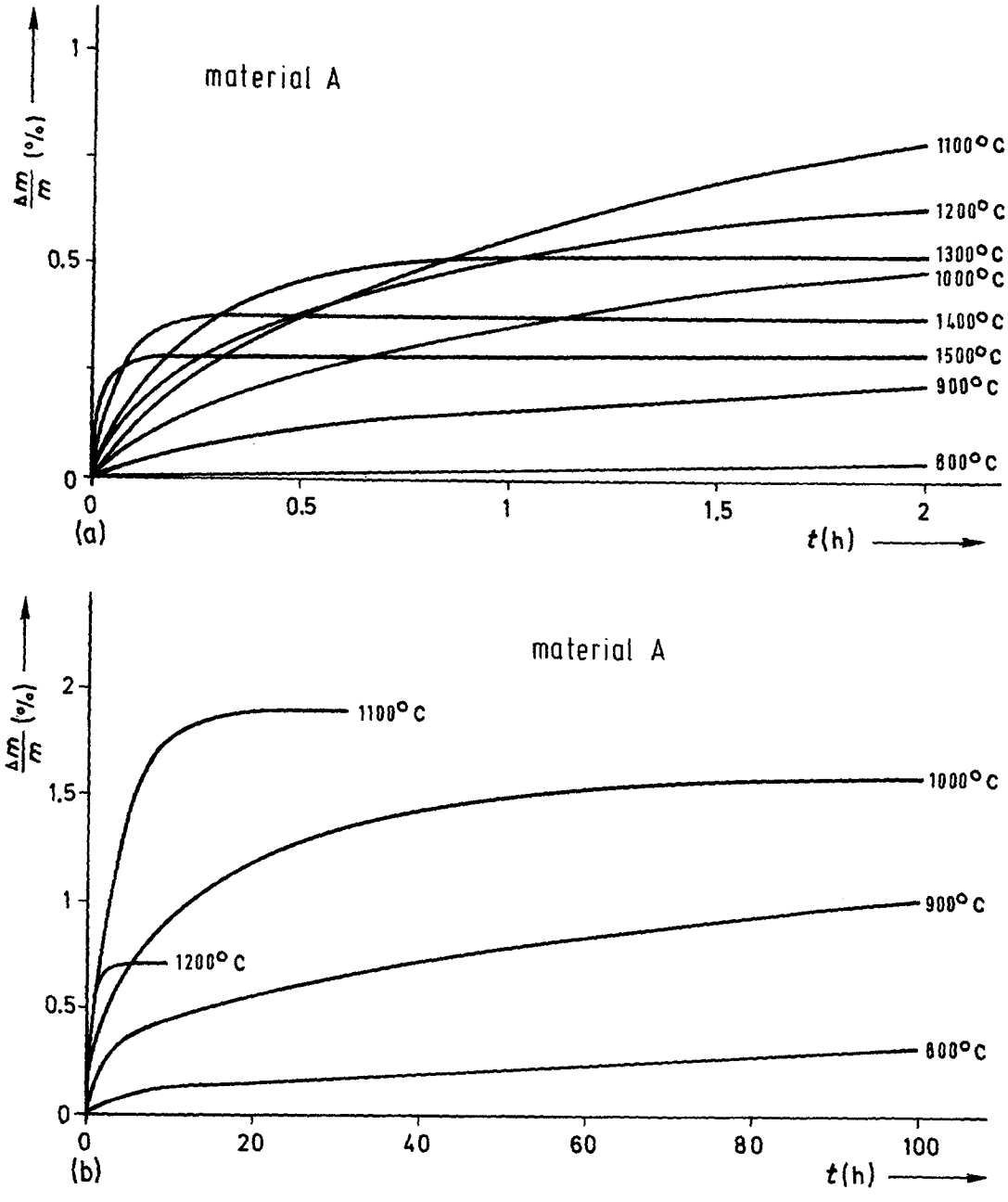

Figure 3 (a) Isothermal oxidation of RBSN in air. (b) Isothermal oxidation of RBSN in air.

dation follows the parabolic relationship in the form

$$\left(\frac{\Delta m}{S}\right)^2 = k_p t \qquad (2)$$

Fig. 5 gives the parabolic plot of the oxidation isotherms for material A in the temperature range 800 to 1000° C. The mass gain is related to the original total internal surface area S_0. At 800° C the oxidation behaviour follows the parabolic law for long times, but at 900 and 1000° C the oxidation isotherms deviate from the straight line towards lower mass gains after 4 and 2 h, respectively. At higher temperatures a parabolic treatment of the oxidation isotherms is no longer possible. The apparent activation energy calculated from the parabolic rate coefficients is 198 kJ mol^{-1}.

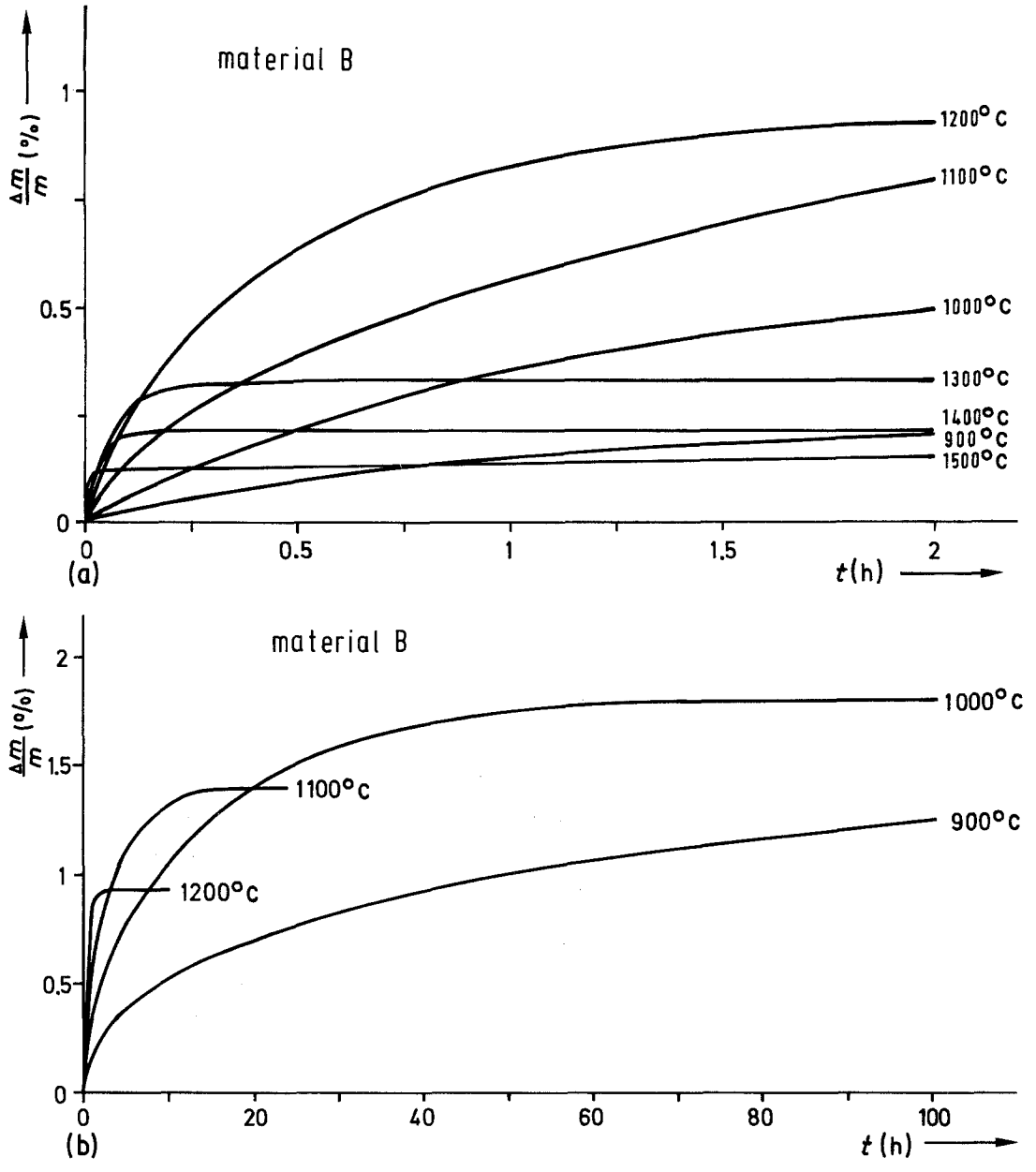

Figure 4 (a) Isothermal oxidation of RBSN in air. (b) Isothermal oxidation of RBSN in air.

3.3. Asymptotic treatment

The typical RBSN oxidation pattern is better represented by an asymptotic treatment of the oxidation isotherms. Evans [27] formulated an asymptotic equation for the case of self-blocking pores, the rate of oxygen uptake being determined by the number of pores still remaining open:

$$\frac{\Delta m}{m} = \frac{\Delta m_\infty}{m}\left[1 - \exp\left(-k_a t\right)\right] \qquad (3)$$

This is a true asymptotic equation, for $\Delta m/m$ can never exceed $\Delta m_\infty/m$, which represents the final mass gain when the horizontal region of the oxidation isotherm is reached; the asymptotic rate coefficient k_a represents a "time constant" to reach this region. When all pores of the RBSN have been closed there still has to be a very low oxidation rate because of the further oxidation at the geometrical surface. For practical purposes this can be neglected compared with the very high initial oxidation rate. In order to get straight lines in the asymptotic drawing of the oxidation iso-

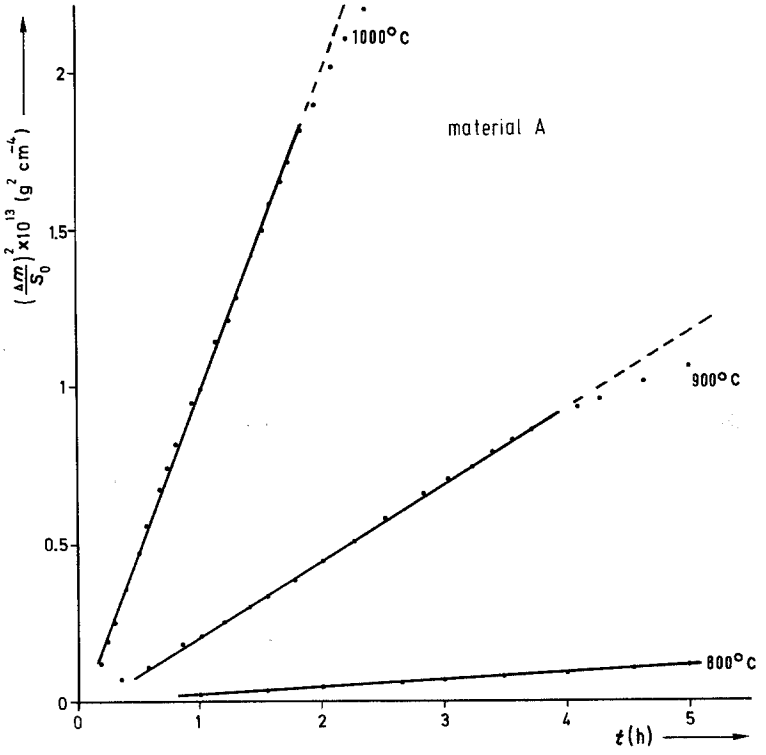

Figure 5 Parabolic plot of mass gain related to the BET surface area of the specimens.

therms one has to rewrite Equation 3 in the form

$$\ln\left(1-\frac{\Delta m}{\Delta m_\infty}\right) = -k_a t \qquad (4)$$

Plotting the left side of this relation against the oxidation time t straight lines are obtained. The slope of these represents the asymptotic rate coefficient. Figs. 6a and b give the asymptotic plots for material A. After the initial parabolic region the oxidation isotherms are very well represented by straight lines. The results of the asymptotic treatment of the RSBN oxidation of both materials are collected in Table II. At the time t_{99}, 99% of the final mass gain are reached, calculated with Equation 3 using the measured k_a values. At temperatures above 1400° C this time is as short as 8 to 20 min. This leads to the fact, that the final mass gain at higher temperature is much lower than at low oxidation temperatures, because the time for internal oxidation with

TABLE II Results of the asymptotic treatment of the oxidation isotherms

Material	Oxidation temperature (° C)	$\frac{\Delta m_\infty}{m}$ (%)	k_a (h^{-1})	time t_{99} $\left(\frac{\Delta m/m}{\Delta m_\infty/m}=0.99\right)$ (min)
A	1000	1.6	0.054	5120
	1100	1.9	0.270	1020
	1200	0.7	1.12	245
	1300	0.5	3.90	71
	1400	0.4	12.8	22
	1500	0.3	30.3	9
B	1000	1.8	0.090	3070
	1100	1.4	0.324	850
	1200	0.9	1.94	140
	1300	0.3	6.98	40
	1400	0.2	17.1	16
	1500	0.15	33.0	8

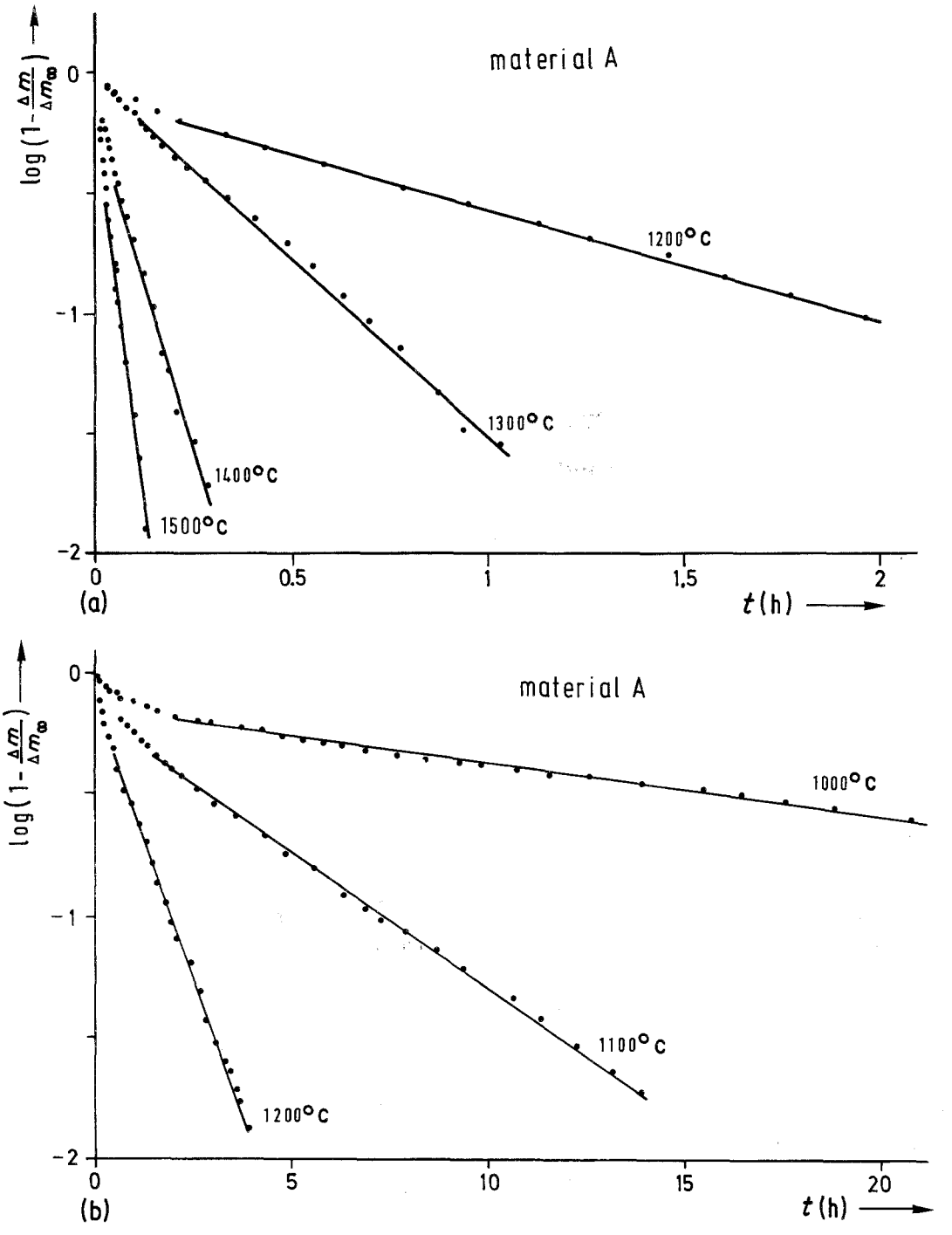

Figure 6 (a) Asymptotic plot of the oxidation isotherms of RBSN. (b) Asymptotic plot of the oxidation isotherms of RSBN.

associated large mass gain is limited. There is a large temperature dependence of the asymptotic rate coefficients as is shown in the Arrhenius plot (Fig. 7). The apparent activation energy is similar for both materials.

4. Mechanism of the RBSN oxidation

4.1. Oxidation model and calculation of reaction depth

The reaction of RBSN with oxygen takes place at both the geometrical and internal surfaces. If

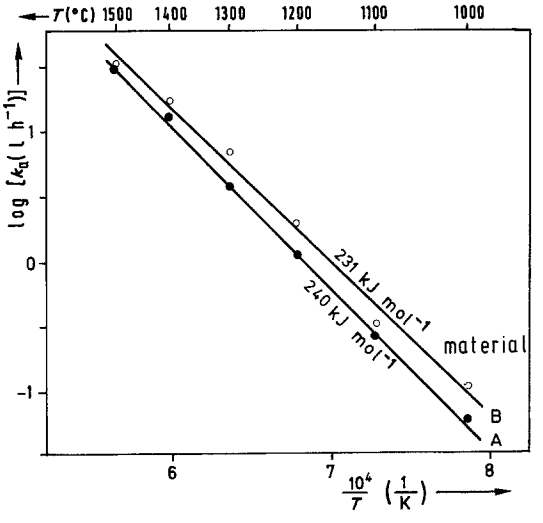

Figure 7 Arrhenius plot of the asymptotic rate coefficient.

enough oxygen is carried into the pores, at any time, they will be completely filled with SiO_2 and large amounts of oxide phases would be formed in the interior of the specimens. This is not the case in practice. This typical oxidation behaviour of RBSN can be described quantitatively as follows.

In the pore channels of RSBN two concurrent processes are active: the diffusive flow of oxygen into the pore volume and the consumption of the oxygen by reaction with Si_3N_4 to form SiO_2. The pore channels in RBSN may be represented by a bundle of parallel cylindrical pore channels of different radii. From this bundle one pore channel with the mean radius r is picked out in Fig. 8 to describe the process of diffusion and simultaneous chemical reaction at the walls of the channel.

At the outer surface of the Si_3N_4 specimen

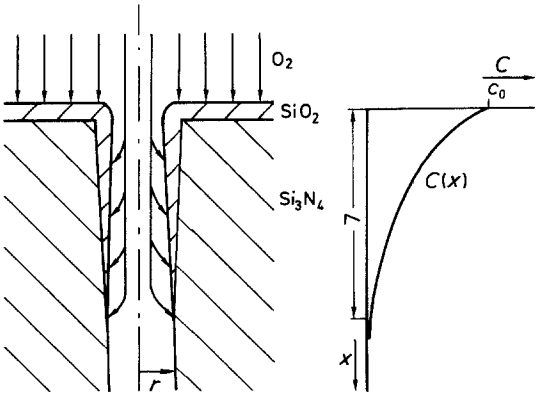

Figure 8 Pore channel model for the discussion of the internal oxidation of RBSN.

there is enough oxygen to produce a homogeneous SiO_2 layer. Inside the pore channel the oxygen concentration is reduced, because of the rapid oxidation reaction. This leads to a concentration profile $c(x)$ with the oxygen concentration c_0 at the pore mouth and c_L at the distance L from the specimen surface. The SiO_2 layer at the channel wall is therefore preferentially thickened in the region of the pore mouth, thus reducing the open diameter of the pore channel.

It is assumed that the oxygen concentration at the outer surface c_0 remains constant, which is justified for tests in flowing air and that there is no forced or free flow along the pore channels. This is fulfilled under practical conditions because the channel radius r is small and the length of the channel is large compared to r. The oxygen concentration in the channel is a function of the axial as well as of the radial coordinates. The concentration change in the radial direction is neglected because r is very small compared to L.

In the steady state, the amount of reactant diffusing into the pore is reacting within the pore. If the time necessary to transport the reactant to the reaction site is smaller than the reaction time, i.e. $t_D < t_R$, the wall of the channel will completely be covered with SiO_2. If this is not the case, only the region near the channel mouth reacts with oxygen. The depth L of the oxidation reaction is determined by the relation

$$t_D = t_R \tag{5}$$

The mean duration for the movement along the distance L is [28]

$$t_D = \frac{L^2}{2D_K} \tag{6}$$

with D_K = Knudsen diffusivity. Because the radii r of the pore channels are extremely small, the mean free path of the oxygen molecules λ being greater than the diameter of the channels, Knudsen flow becomes effective. The expression for the Knudsen diffusivity is [29]

$$D_K = \tfrac{4}{3} r \left(\frac{2RT}{\pi M}\right)^{1/2} \tag{7}$$

where R is the gas constant, T absolute temperature and M is the molecular mass of the transported species.

The mean duration of the reaction is calculated from the time necessary to react all the oxygen in the channel. There are $\pi r^2 L \bar{c}$ mol present, with

TABLE III Calculated depth of reaction zone and mass gain for the RBSN oxidation

Temperature (° C)	Knudsen diffusivity in material ($cm^2 sec^{-1}$)		Oxidation rate coefficient		Depth of reaction zone in material (mm)		Mass gain for material (%)	
	A	B	linear ($cm\,sec^{-1}$) $\times 10^9$	parab. ($cm^2 sec^{-1}$) $\times 10^{14}$	A	B	A	B
1000	0.66	0.31	0.17	0.66	4.70	2.20	7.7	2.3
1100	0.68	0.32	1.17	1.80	1.75	0.82	2.9	0.8
1200	0.71	0.33	5.90	4.40	0.77	0.36	1.3	0.4
1300	0.73	0.34	21.7	9.40	0.39	0.18	0.6	0.2
1400	0.75	0.35	78.0	18.00	0.20	0.09	0.3	0.1
1500	0.78	0.36	240.0	33.00	0.12	0.05	0.2	0.05

the mean oxygen concentration $\bar{c} = 0.2 c_0$ [3]. This is enough to form a SiO_2 layer of the thickness $d_{SiO_2} = (\bar{c}rM)/(2\rho)$. M is the molecular mass of oxygen and ρ the density of SiO_2 ($= 2.2\,g\,cm^{-3}$). For simplicity a flat geometry with the initial channel wall area being constant is assumed. With the linear parabolic rate law (Equation 1) substituting the mass gain per unit area by the thickness of the SiO_2 layer, t_R becomes

$$t_R = d_{SiO_2}\left(\frac{d_{SiO_2}}{k_p} + \frac{1}{k_l}\right) = \frac{\bar{c}rM}{2\rho}\left(\frac{\bar{c}rM}{2\rho}\frac{1}{k_p} + \frac{1}{k_l}\right) \quad (8)$$

Thus with Equation 5 the relation for the depth of reaction can be written in the form

$$L = \left[D_K \frac{\bar{c}rM}{\rho}\left(\frac{\bar{c}rM}{\rho}\frac{1}{2k_p} + \frac{1}{k_l}\right)\right]^{1/2} \quad (9)$$

The final mass gain can be calculated approximately, assuming the channels have been completely closed near the mouth, and the SiO_2 profile in the bulk of the specimens following the oxygen concentration profile along the channel axis. The area S at the mouth of the channels which has to be filled with SiO_2 is

$$S = \epsilon S_G \zeta \quad (10)$$

where ϵ is the open porosity, S_G is the geometric surface area of the specimen and ζ ($= 2.2$) is a factor which takes into account that the volume of SiO_2 formed is greater than the volume of Si_3N_4 consumed. To get the SiO_2 volume, Equation 10 has to be multiplied by the depth of reaction L and the ratio $\chi = 0.2$ for the concentration profile. This leads to the SiO_2 mass formed during oxidation

$$m = \rho \epsilon S_G \zeta L \chi \quad (11)$$

In Table III the Knudsen diffusivity and the linear and parabolic Si_3N_4 oxidation-rate coefficients are listed together with the calculated depth of reaction and the final mass gain for the two RBSN materials in the temperature range 1000 to 1500° C. The oxidation rate-coefficients have been taken from the work of Tétard *et al.* [5]. The pronounced temperature dependence of the depth of reaction and thus the mass gain results from the fact that the Knudsen diffusivity is only increased with the square root of the temperature, whilst the rate coefficient increases exponentially.

4.2. Comparison with experimental data

The profile of oxide phases in RSBN has been determined using several methods of analysis as has been already described [23]. It was shown that the cristobalite profile determined by X-ray diffraction gives a representative picture of the amount of internal oxidation. Figs. 9 and 10 give cristobalite profiles in oxidized specimens of both RBSN qualities. These figures clearly show, that, in the RBSN qualities used, only a small zone beneath the surface is attacked by the oxygen. The depth of this zone corresponds for higher temperatures with the calculated data in Table III. For low temperatures there is a discrepancy towards larger calculated values. This may result from the presence of amorphous SiO_2 phase, which has not been converted to cristobalite and from the detection limit of X-ray analysis. In addition, for longer oxygen transportation distances in the pore channels, tortuosity effects may reduce the capability for oxygen transport.

Porosimetry measurements have been performed with oxidized specimens. Diagrams for specimens oxidized at 1260° C for different times are shown in Figs. 11 and 12. Obviously, the surface of the specimens have not been fully glazed

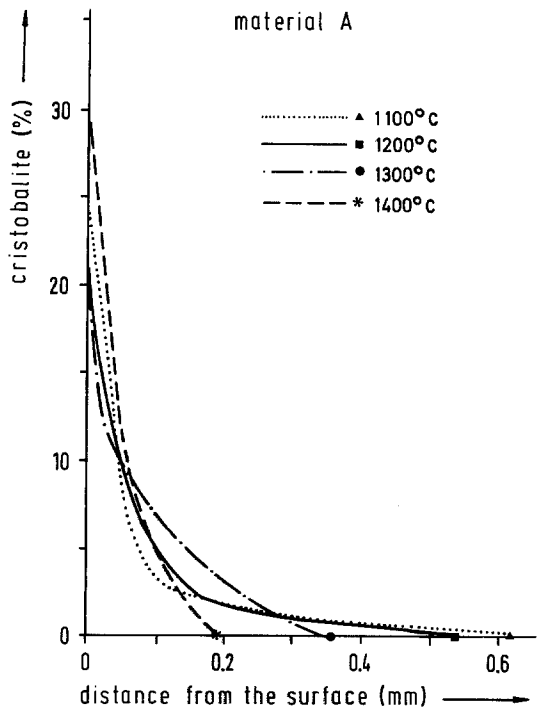

Figure 9 Profiles of cristobalite in RBSN after oxidation.

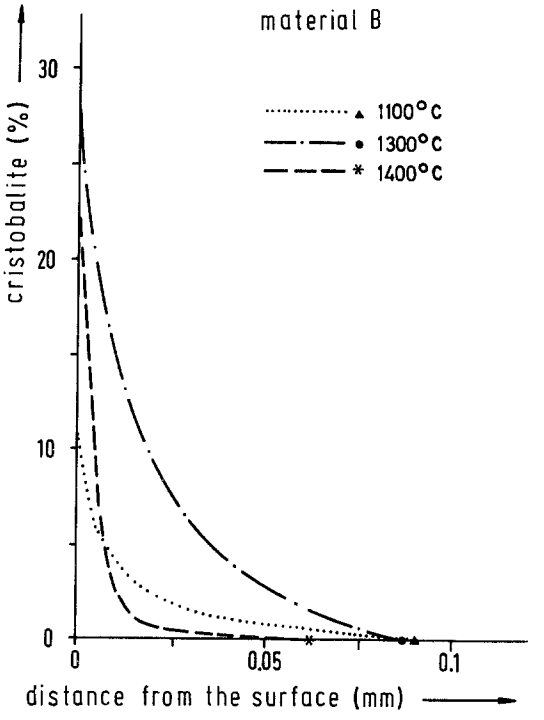

Figure 10 Profiles of cristobalite in RBSN after oxidation.

with SiO_2, since 60 to 75% of the initial open porosity is still open and could be filled with mercury. The intrusion curves are shifted towards smaller radii and with increasing oxidation time more mercury is trapped because the pore channels are narrowed near the mouth. The results of the mercury porosimetry tests are collected in Table IV. The mean pore channel radii after oxidation reach values of 12 to 20 nm compared to 50 and 108 nm before oxidation.

The specific surface area of the specimen is diminished with oxidation time. Measurements of the specific surface after oxidation revealed that, in spite of reaching the final mass gain, up to 70% of the initial specific surface area is accessible to nitrogen.

5. Conclusions

The oxidation of RBSN is extremely sensitive to the amount and type of open porosity. An essen-

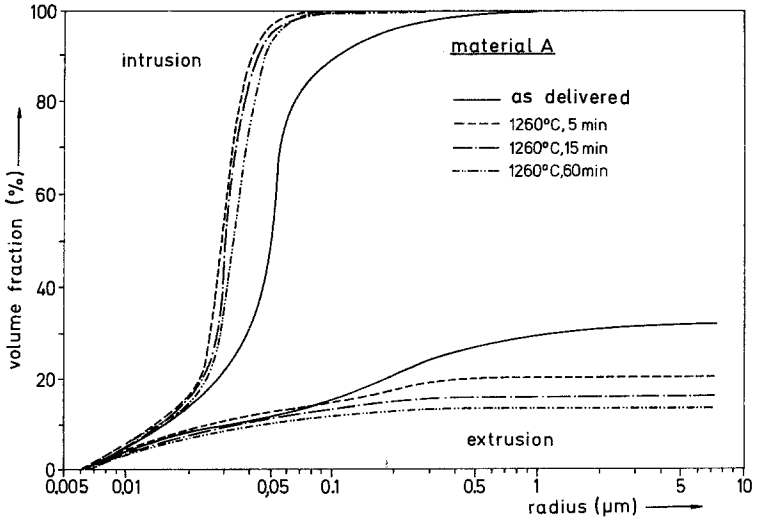

Figure 11 Distribution of open porosity in RBSN after oxidation.

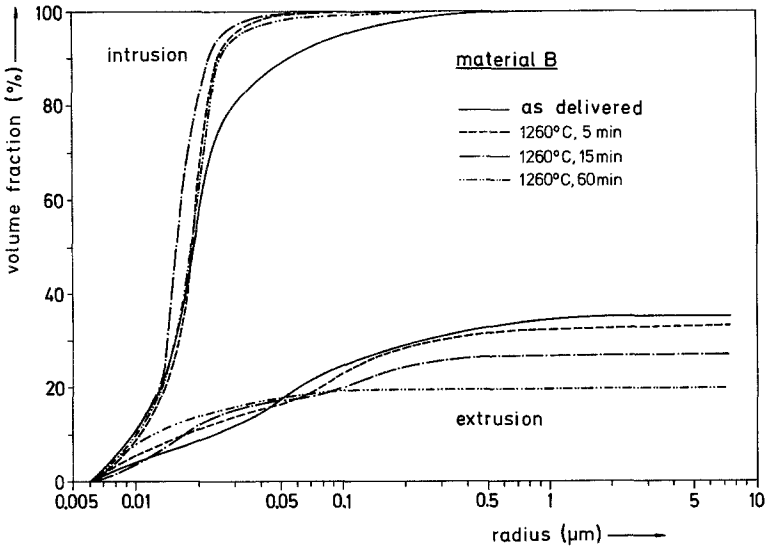

Figure 12 Distribution of open porosity in RBSN after oxidation.

tial requirement for small amounts of internal oxidation products is to limit the pathways for oxygen penetration into the interior of the specimens. This can be achieved with RBSN materials containing very small pore channels. In these channels two concurrent processes are active: the diffusion of oxygen along the channel axis and the reaction of oxygen with Si_3N_4 at the walls of the channels to form SiO_2. Since the diameter of the pore channels is less than the mean free path of the oxygen molecules, the diffusion follows the conditions of Knudsen flow. Because of the high oxidation reaction rate and only limited possibility for oxygen transport into the pore channels, the oxidation reaction is limited only to an outer part of the pore channels. With raising temperature this reaction zone is reduced rapidly because of the exponential increase of the reaction rate and only the square root dependence of Knudsen diffusivity on temperature. The knowledge of diffusion, reaction, and porosity data allows to estimate the depth of the reaction zone and the mass gain for the RBSN-oxidation at different temperatures. The results showed that the mean pore channel radius, determined by mercury porosimetry, is a realistic tool for the quantitative description of the oxidation behaviour of RBSN, inspite of several uncertainties of the mercury porosimetry [25] and some simplifying assumptions in the calculation of the reaction depth.

It was shown by the oxidation model applied and confirmed by the post oxidation investigations of the specimens that the limitation of oxidation to the outer zone of the RBSN is primarily due to

TABLE IV Results of mercury porosimetry of oxidized specimens

Material	Oxidation conditions		Fraction of trapped mercury (%)	Mean pore channel radius (nm)
	T (° C)	t (min)		
A	–	–	68	108
	1000	15	82	45
		1440	86	20
	1260	5	80	28
		15	84	23
		60	86	19
B	–	–	64	50
	1000	15	68	50
		60	80	26
		6000	85	18
	1260	5	63	40
		15	73	23
		60	80	12

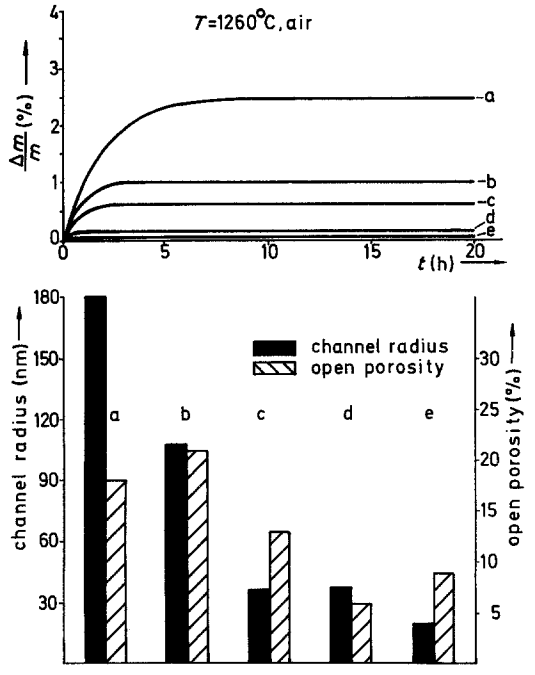

Figure 13 Oxidation of 5 RBSN-qualities ($\rho \approx 2.6\,g\,cm^{-3}$) with different pore characteristics.

the concurrent diffusion and reaction processes. It is not necessary that all the pores are sealed with SiO_2 via viscous flow of SiO_2 into the pores or preferential crystallization at the pore mouth as has been discussed in literature [6, 17].

The results clearly indicate, that high quality RBSN may well be used in oxidizing atmospheres without extensive internal oxidation, provided the pore channel radii are small. This is undoubtedly confirmed in Fig. 13, where the oxidation isotherms at 1200° C for 5 RBSN materials are plotted together with their porosity data. Although the density of the 5 materials is nearly equal ($\sim 2.6\,g\,cm^{-3}$), the oxidation differs considerably and the mass gain can directly be related to the mean pore channel radius.

RBSN qualities are now available with a density of about 2.6 to $2.7\,g\,m^{-3}$ and open porosity of less than 10% consisting of pore channels with mean radii of 20 to 30 nm. The mass gain after 3000 h oxidation in air of such RBSN qualities is about 1% at 1000° C and about 0.3% at 1260° C oxidation temperature.

Acknowledgements

This work has been carried out at the University of Karlsruhe with the support of the Bundesministerium für Forschung und Technologie, Bundesrepublik Deutschland. The authors wish to thank their colleagues at the institute for many helpful discussions and experimental assistance, especially Mrs G. Braun for porosity measurement and the group of Mrs Dr. Ch. Adelhelm (Kernforschungszentrum) for the chemical analysis.

References

1. G. GRATHWOHL and F. THÜMMLER, *J. Mater. Sci.* **13** (1978) 1177.
2. F. PORZ, G. GRATHWOHL and F. THÜMMLER, *Proc. Brit. Ceram. Soc.* **31** (1981) 157.
3. F. PORZ, "Reaktionsgesintertes Siliziumnitrid: Charakterisierung, Oxidation and mechanische Eigenschaften" Report KfK 3375 (1982).
4. R. M. HORTON, *J. Amer. Ceram. Soc.* **52** (1969) 121.
5. D. TÉTARD, P. LORTHOLARY, P. GOURSAT and M. BILLY, *Rev. Int. Htes. Temp. Réfract.* **10** (1973) 153.
6. R. EBI, Diss., Universität Karlsruhe (1973).
7. M. MITOMO and J. H. SHARP, *Yogyo-Kyokai-Shi* **84** (1976) 33.
8. J. MUKERJI and A. K. NANDI, *Ind. J. Technol.* **16** (1978) 419.
9. I. FRÄNZ and W. LANGHEINRICH, *Solid-State Electron.* **14** (1971) 499.
10. J. H. ROSOLOWSKI and C. D. GRESKOVICH, "Ceramic Sintering", Report G.E.Co. (1974) SRD-74-116, AD/A-00 1012.
11. F. S. GALASSO, R. D. VELTRI and W. J. CROFT, *Amer. Ceram. Soc. Bull.* **57** (1978) 453.
12. T. HIRAI, K. NIIHARA and T. GOTO, *J. Amer. Ceram. Soc.* **63** (1980) 419.
13. L. V. CHRAMOVA, T. P. SMIRNOVA, A. B. AYUPOV and V. I. BELYI, *Thin Solid Films* **78** (1981) 303.
14. H. A. SCHAEFFER, "Sauerstoff- und Siliciumdiffusion in silicatischen Gläsern". Habilitationsschrift Universität Erlangen-Nürnberg (1980).
15. J. F. COLLINS and R. F. GERBY, *J. Met.* **7** (1955) 612.
16. A. M. SAGE and J. H. HISTED, *Powder Metall.* **4** (1961) 196.
17. R. W. DAVIDGE, A. G. EVANS, D. GILLING and P. R. WILYMAN, in "Special Ceramics 5", edited by P. Popper (British Ceramic Research Association, Manchester, 1972) p. 329.
18. I. Y. GUZMAN, Y. N. LITVIN and G. V. TURCHINA, *Refractories* **15** (1974) 118.
19. M. E. WASHBURN and H. R. BAUMGARTNER, in "Ceramics for High Performance Applications", edited by J. J. Burke, A. E. Gorum and R. N. Katz (Brook-Hill, Chestnut Hill MA, 1974) p. 479.
20. B. D. KRUSE, G. WILLMANN and H. HAUSNER, *Ber. dt. Keram. Ges.* **53** (1976) 349.
21. J. MUKERJI, A. K. NANDI and K. K. DHARGUPTA, *Glass Ceram. Bull. (Calcutta)* **25** (1978) 55.
22. J. B. WARBURTON, J. E. ANTILL and R. W. M.

HAWES, *J. Amer. Ceram. Soc.* **61** (1978) 67.
23. G. GRATHWOHL, F. PORZ and F. THÜMMLER, *Proc. Brit. Ceram. Soc.* **26** (1978) 129.
24. P. BARLIER and J. P. TORRE, *J. Mater. Sci.* **14** (1979) 235.
25. H. COHRT, F. PORZ and F. THÜMMLER, *Powder Metall. Int.* **13** (1981) 121.
26. B. E. DEAL and A. S. GROVE, *J. Appl. Phys.* **36** (1965) 3770.
27. U. R. EVANS, "The Corrosion and Oxidation of Metals" (Edward Arnold, London, 1960) p. 834.
28. A. EINSTEIN, *Ann. Phys.* **17** (1905) 549.
29. E. E. PETERSEN, "Chemical Reaction Analysis" (Prentice-Hall, Englewood Cliffs, NJ, 1965) p. 115.

Received 4 July
and accepted 26 July 1983